Photoionization cross section and resonance structure of atomic yttrium

Wasantha Wijesundera and Hugh P. Kelly
Department of Physics, University of Virginia, Charlottesville, Virginia 22901
(Received 26 March 1987)

Many-body perturbation theory has been used to calculate the photoionization cross section of neutral yttrium from threshold at 6.52–100.0 eV. The resonance structure due to $4p$ excitations to $4d$ states has also been calculated. Hartree-Fock results are also presented for comparison.

I. INTRODUCTION

In the transition-metal elements there has been extensive observation of very interesting resonance structure due to $3p \rightarrow 3d$ transitions.[1–10] However, there have been no comparable measurements published for atoms with configuration $4p^6 4d^N 5s^2$ in the next row of the Periodic Table, although data for the solid do exist.[11] We would expect the resonance structure due to $4p \rightarrow 4d$ excitations in such elements to be at least as interesting as that in the transition-metal elements. The measured photoionization cross section for solid yttrium does show a broad peak.[11] Recently the resonance structure for atomic yttrium has been observed by Mansfield.[12]

In this paper we present a detailed calculation of the photoionization cross section of the neutral yttrium atom in the $4p^6 5s^2 4d(^2D)$ ground state for photon energies ranging from threshold at 6.52–100.0 eV. The effect of resonances due to $4p$ excitations is included. The calculations were carried out in LS coupling, and spin-orbit splitting effects and relativistic effects were not considered. The effective single-particle potential introduced by Qian *et al.*[13] was used to calculate some of the continuum channels. The calculations used many-body perturbation theory (MBPT) (Refs. 14–16) and our coupled-equations method[17] to account for interactions between different channels in the final state. The coupled-equations method is a technique in which the integral equations account for interaction to all orders between different channels with the same total L and S. This is equivalent to the K-matrix method.[18] Our final-state channels only included those in which there is a single excitation. Therefore our calculations do not show double-electron-resonance structure.

Section II includes the theoretical details of our method. We present results of the calculation in Sec. III, and conclusions are contained in Sec. IV.

II. THEORY AND METHODS

In this work MBPT is used to calculate dipole length and velocity transition matrix elements. We begin with the Hamiltonian

$$H = H_0 + H_C \ , \tag{1}$$

where

$$H_0 = \sum_{i=1}^{N} \left[-\tfrac{1}{2}\nabla_i^2 - \frac{Z}{r_i} + V(r_i) \right] , \tag{2}$$

and

$$H_C = \sum_{\substack{i,j=1 \\ (i<j)}}^{N} v_{ij} - \sum_{i=1}^{N} V(r_i) \ . \tag{3}$$

Atomic units are used throughout the paper. The term v_{ij} represents the Coulomb interaction between electrons i and j. The single-particle potential $V(r_i)$ accounts for the average interaction of the ith electron with the remaining $N-1$ electrons.

Dipole matrix elements are required to calculate photoionization cross sections. The dipole length matrix elements are given by

$$Z_L(p \rightarrow k) = \left\langle \psi_f \left| \sum_{i=1}^{N} z_i \right| \psi_0 \right\rangle , \tag{4}$$

where ψ_0 and ψ_f are many-particle ground and excited states. The final state ψ_f results from the excitation of an electron from the ground-state orbital p to the excited-state orbital k. The dipole velocity form is expressed as

$$Z_V(p \rightarrow k) = \frac{1}{E_0 - E_k} \left\langle \psi_f \left| \sum_{i=1}^{N} \frac{d}{dz_i} \right| \psi_0 \right\rangle , \tag{5}$$

where E_0 and E_k are energy eigenvalues corresponding to ψ_0 and ψ_f. The velocity and length forms are equal for exact eigenstates of H.

The continuum kf and kp states of

$$4p^6 5s^2 kf(^2F),\ 4p^6 5s^2 kp(^2P) \ ,$$

$$4p^6 5s 4d(^3D) kp(^2F),\ 4p^6 5s 4d(^1D) kp(^2F) \ ,$$

$$4p^6 5s 4d(^3D) kp(^2D),\ 4p^6 5s 4d(^1D) kp(^2D) \ ,$$

$$4p^6 5s 4d(^3D) kp(^2P),\ 4p^6 5s 4d(^1D) kp(^2P)$$

were calculated in the respective Hartree-Fock potentials. If the Hartree-Fock potential is used to calculate the continuum kd states which results from the excitation of an electron from the $4p^6$ subshell, one must calculate eighteen different radial wave functions corresponding to eighteen possible channels. However, a sin-

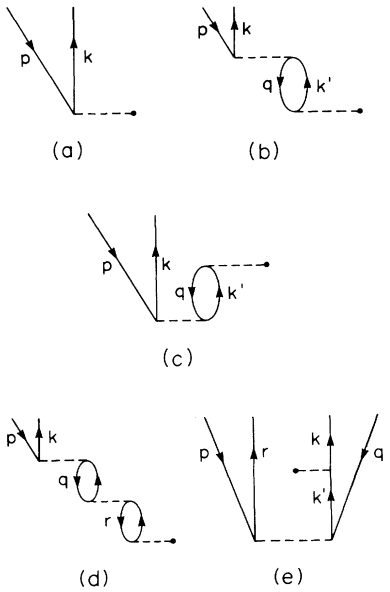

FIG. 1. Figures contributing to the matrix element Z $(p \rightarrow k)$. Dashed lines ending with a solid dot indicate matrix elements of Z. The other dashed lines represent Coulomb interactions. Figure 1(a) depicts the lowest-order dipole matrix element for the transition $p \rightarrow k$. Figure 1(b) shows a final-state correlation to first order in H_C and Fig. 1(d) shows coupling among three final-state channels. The ground-state correlations to the first order in H_C are shown in Figs. 1(c) and 1(e).

gle set of radial wave functions for kd states (due to $4p \rightarrow kd$ excitations) was calculated by using the effective potential introduced by Qian *et al.*[13] The effective single-particle potential averaged over M_L and M_S is given by[13]

$$V_{LS\text{av}} = \frac{1}{2L+1} \sum_{M_L,F} \frac{V_F \, | \langle F \, | \, Z \, | \, G \rangle \, |^2}{\sum_F | \langle F \, | \, Z \, | \, G \rangle \, |^2} , \tag{6}$$

where

$$\langle F \, | \, V_F \, | \, F \rangle = \sum_I \frac{\langle F \, | \, V \, | \, I \rangle \langle I \, | \, Z \, | \, G \rangle}{\langle F \, | \, Z \, | \, G \rangle} . \tag{7}$$

TABLE I. Threshold energies for $4p$ ionization

Ionic Core	ΔSCF (eV)[a]	Corrected threshold (eV)[b]
$4p^5 5s^2 4d\,(^3F)$	31.72	32.85
$4p^5 5s^2 4d\,(^1F)$	33.53	34.69
$4p^5 5s^2 4d\,(^3D)$	33.44	34.54
$4p^5 5s^2 4d\,(^1D)$	33.44	34.54
$4p^5 5s^2 4d\,(^3P)$	30.72	31.83
$4p^5 5s^2 4d\,(^1P)$	38.20	39.17

[a]Difference between ionic core level and ground state $4p^6 5s^2 4d$.
[b]The calculated second-order excited-state correlations and estimated pair correlation energies among $4p$ and $4d$ electrons were added to the ΔSCF value.

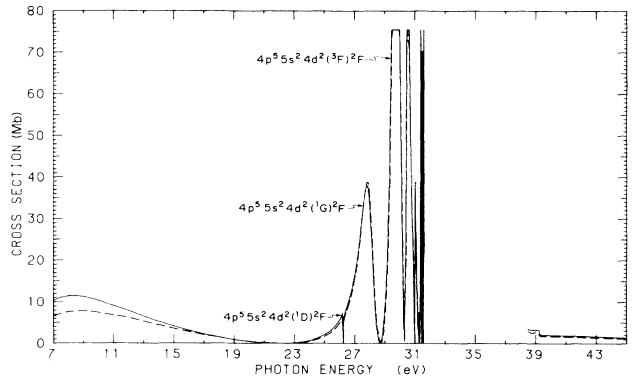

FIG. 2. Partial photoionization cross sections in dipole length (solid line) and dipole velocity (dashed line) formalism for $4p^6 5s^2 4d\,(^2D) \rightarrow 4p^6 5s^2 kf\,(^2F)$. The dense region of Rydberg resonances which lies between 31.10 and 39.70 eV is not shown.

The state $| G \rangle$ represents the LS-coupled ground state, $| F \rangle$ represents one of the final states of interest, and $| I \rangle$ represents any channel which has the same orbital angular momentum for the continuum electron. For example, if $| G \rangle$ and $| F \rangle$ represent the ground state $4p^6 5s^2 4d\,(^2D)$ and the final state $4p^5 5s^2 4d\,(^3F) kd\,(^2F)$, respectively, then states $| I \rangle$ which contribute to the sum in Eq. (7) are

$$4p^5 5s^2 4d\,(^3F) kd\,(^2F),\ 4p^5 5s^2 4d\,(^1F) kd\,(^2F) ,$$

$$4p^5 5s^2 4d\,(^3D) kd\,(^2F),\ 4p^5 5s^2 4d\,(^1D) kd\,(^2F) ,$$

$$4p^5 5s^2 4d\,(^3P) kd\,(^2F),\ 4p^5 5s^2 4d\,(^1P) kd\,(^2F) .$$

The states $| I \rangle$ differ among themselves only in having different values of L,S for the $4p^5 4d\,(LS)$ coupling and the state $| F \rangle$ is included in the sum over states $| I \rangle$. Equation (7) is only used to obtain the factors multiplying direct and exchange terms in the potential V_F. This

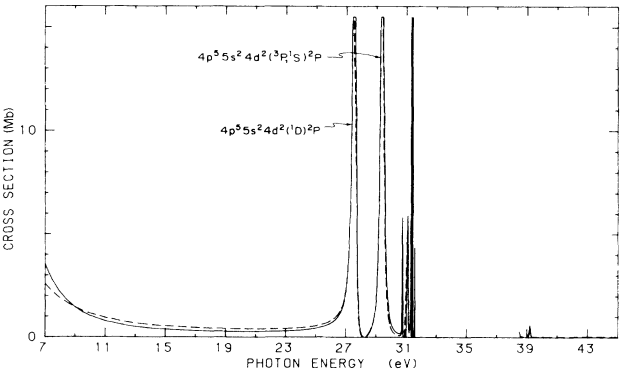

FIG. 3. Partial photoionization cross sections in dipole length (solid line) and dipole velocity (dashed line) formalism for $4p^6 5s^2 4d\,(^2D) \rightarrow 4p^6 5s^2 kp\,(^2P)$. The dense region of Rydberg resonances which lies between 31.10 and 39.70 eV is not shown.

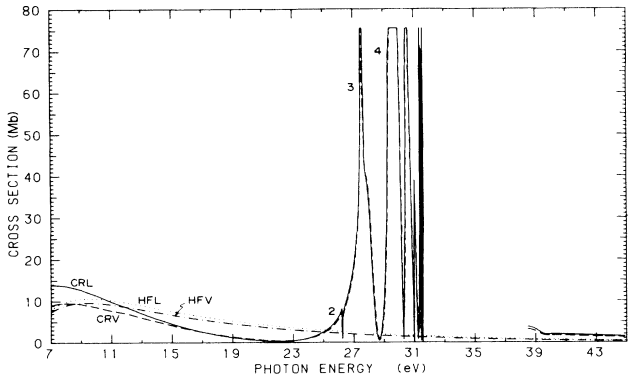

FIG. 4. Hartree-Fock and correlated $4d$ total cross sections. HFL and HFV are Hartree-Fock length and velocity cross sections, respectively. CRL and CRV are correlated length and velocity cross sections, respectively. The dense region of Rydberg resonances which lies between 31.10 and 39.70 eV is not shown. The numbered resonances are given in Table III.

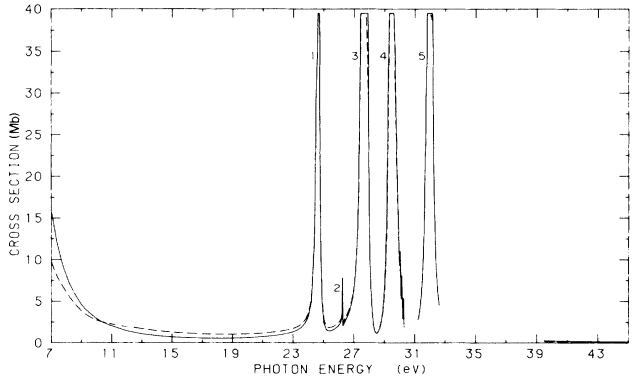

FIG. 5. The correlated $5s$ total cross sections in dipole length (solid line) and dipole velocity (dashed line) formalism. The dense region of Rydberg resonances which lies between 31.10 and 39.70 eV is not shown. Only the $4p^5 5s^2 4d^2(^3F)^2D$ resonance at 32.00 eV is shown. The numbered resonances are given in Table III.

potential is discussed in more detail in Ref. 13, where it was shown to be very useful in accounting for final-state interactions for chlorine. A similar potential was used to calculate ks states which also result from the excitation of an electron from the ground-state orbital $4p$. The use of $V_{LS\mathrm{av}}$ of Eq. (6) includes the effects of final-state interactions in an approximate way between channels which involve the same angular momentum of the continuum electron and excitation of a bound orbital from the same subshell. Radial $4d$ orbitals were calculated both in the ground state and in the self-consistent Hartree-Fock approximation of excited cores $4p^5 5s^2 4d^2(^3F)$, $4p^5 5s^2 4d^2(^3P)$, $4p^5 5s^2 4d^2(^1D)$, $4p^5 5s^2 4d^2(^1G)$, and $4p^5 5s^2 4d^2(^1S)$. The overlaps between $4d$ and $kd\,(nd)$ states were taken into account.

The diagrams contributing to $Z(p \rightarrow k)$ are shown in Fig. 1. The exchange diagrams are not shown but were included. Figure 1(a) depicts the lowest-order dipole matrix element for the transition $p \rightarrow k$. Figure 1(b) shows a final-state correlation to first order in H_C in which excitation $q \rightarrow k'$ are coupled to the $p \rightarrow k$ excitations and Fig. 1(d) shows coupling among three final-state channels, namely, p, q, and r. The ground-state correlations to first order in H_C are shown in diagrams 1(c) and 1(e). Figure 1(e) does not contribute for closed-shell atoms, but does contribute for open-shell atoms when r represents an open subshell (for example, $4d$ subshell in yttrium). More details about Figs. 1(a)–1(e) may be found in previous papers.[19,20]

The coupled-equations method[17] was used to couple the interactions between all possible single-particle excitation channels to all orders in perturbation theory. When we coupled the interactions between channels which result from $4p \rightarrow nd,kd$ (or $4p \rightarrow ns,ks$) excitations, for the intrachannel couplings, the differences between the effective potentials of Eq. (6) and the channel Hartree-Fock potentials were included in the coupled equations. This ensures the cancellation of two-electron (Coulomb) interactions between $4p^5 5s^2 4dkd$ and $4p^5 5s^2 4dk'd$ states, which belong to the same channel, by interactions with the potential $V(r_i)$ in Eq. (3).[21]

The photoionization threshold energies were taken from experiment[22] for $4d$ and $5s$ excitations. For $4p$ excitations we determined the difference of self-consistent-

TABLE II. Comparison of length and velocity $4d$ photoionization cross sections at higher energies. The total cross section (the sum of $4p^6 5s^2 kf$ and $4p^6 5s^2 kp$ partial cross sections) is given in megabarns. The symbols L and V refer to length and velocity formalism.

	Hartree Fock		Coupled equations	
ω (eV)	L	V	L	V
224.22	0.029 60	0.025 43	0.041 73	0.046 68
496.34	0.006 76	0.006 07	0.007 17	0.007 43
877.30	0.001 80	0.001 47	0.002 08	0.001 98
1965.76	0.000 13	0.000 14	0.000 16	0.000 16

TABLE III. Positions of $4p \rightarrow 4d$ resonances.

Line No.[a]	Resonance	Position (eV)[b]
1	$4p^5 5s^2 4d^2(^3P)^2D$	24.65
2	$4p^5 5s^2 4d^2(^1D)^2F$	26.20
3	$4p^5 5s^2 4d^2(^1D)^2P$	27.50
3	$4p^5 5s^2 4d^2(^1G)^2F$	27.80
3	$4p^5 5s^2 4d^2(^1D)^2D$	27.80
4	$4p^5 5s^2 4d^2(^3P)^2P$	29.40
4	$4p^5 5s^2 4d^2(^1S)^2P$	29.40
4	$4p^5 5s^2 4d^2(^3F)^2F$	29.70
5	$4p^5 5s^2 4d^2(^3F)^2D$	32.00

[a]These numbers are used to identify resonances shown in Figs. 4, 5, and 7.

[b]The positions above the ground state $4p^6 5s^2 4d$ were calculated by adding the second-order excited-state correlations and estimated pair correlation energies among $4p$ and $4d$ electrons to the ΔSCF values.

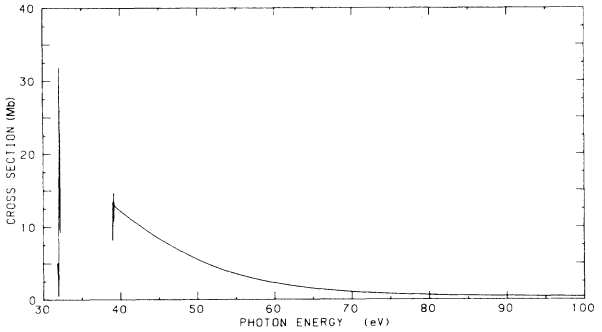

FIG. 6. The correlated $4p$ total cross sections in dipole length formalism. The velocity results are very close to the length results. The dense region of Rydberg resonances which lies between 31.10 and 39.70 eV is not shown. Note that the cross section begins at 31.10 eV and the effects of Rydberg resonances at threshold can be seen.

field Hartree-Fock calculations[23] (ΔSCF), and we also estimated roughly the breaking of pair correlation energies[24] among $4p$ and $4d$ electrons when one $4p$ electron is excited by using the corresponding correlations among $3p$ electrons calculated by Kelly and Ron.[25] These corrections were added to the ΔSCF values. As seen from Table I, these effects contribute approximately 1 eV to the ionization energy of a $4p$ electron. In our calculation, the only effect from such pair correlations is the ($\sim$1 eV) shifts in ionization thresholds and resonances and is not expected to affect the shape of the cross section. These shifts appear to bring the resonance positions into better agreement with those measured by Mansfield.[12] However, explicit calculation of correlations in the $4p$ subshell would be useful, and we plan to undertake this project in the future.

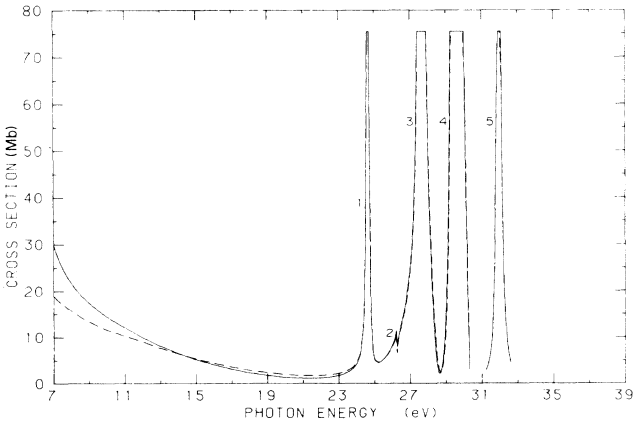

FIG. 7. The correlated total cross sections (sum of $4d$, $5s$, and $4p$ cross sections) in dipole length (solid line) and dipole velocity (dashed line) formalism. The dense region of Rydberg resonances which lies between 31.10 and 39.70 eV is not shown. Only the $4p^5 5s^2 4d^2(^3F)^2D$ resonance at 32.00 eV is shown. The numbered resonances are given in Table III.

III. RESULTS

We show our results for the $4p^6 5s^2 kf$ cross sections in both dipole length and velocity approximations in Fig. 2. Near threshold (6.53–6.8 eV) there are excitations $5s \rightarrow np$ ($n \geq 5$) which are degenerate with $4d \rightarrow kf$ excitations and give rise to resonances. (The threshold energies corresponding to $4p^6 5s 4d(^3D)$ and $4p^6 5s 4d(^1D)$ ionic cores are 6.67 and 6.94 eV, respectively.) However, the overall effect from these is weak and not shown. The cross section, which has a maximum at 8.0 eV, gradually decreases and then begins to increase due to $4p \rightarrow 4d$ resonances. The peak at 26.20 eV is due to the resonance $4p^6 5s^2 4d \rightarrow 4p^5 5s^2 4d^2(^1D)^2F$. The resonances due to $4p^6 5s^2 4d \rightarrow 4p^5 5s^2 4d^2(^1G)^2F$ and $4p^6 5s^2 4d \rightarrow 4p^5 5s^2 4d^2(^3F)^2F$ excitations have peaks at 27.80 and 29.70 eV. These three peaks in Mb are 7.36 (6.89), 37.95 (38.94), and 154.47 (152.10) in length (velocity) form. Other large resonances are $4p^5 5s^2 4d(^3P)5d(^2F)$ and $4p^5 5s^2 4d(^3F)6s(^2F)$ both at 30.50 eV and $4p^5 5s^2 4d(^3P)6d(^2F)$ at 31.10 eV. In the range 31.0–39.70 eV we find resonances due to $4p \rightarrow nd$ ($n \geq 5$) and $4p \rightarrow ns$ ($n \geq 6$) excitations which are degenerate in energy with $4d \rightarrow kf$ excitations. Since our main purpose is to investigate the resonance structure due to $4p \rightarrow 4d$ excitations we do not show all the resonances due to $4p \rightarrow nd, ns$ excitations.

We present our results for $4p^6 5s^2 kp$ length and velocity cross sections in Fig. 3. These are much smaller than the $4p^6 5s^2 kf$ cross sections. The resonance at 27.50 eV is $4p^5 5s^2 4d^2(^1D)^2P$. Both $4p^5 5s^2 4d^2(^3P)^2P$ and $4p^5 5s^2 4d^2(^1S)^2P$ resonances peak at 29.40 eV. These two peaks, in length (velocity), are 66.98 Mb (61.40 Mb) and 285.18 Mb (254.06 Mb) respectively. Other resonances of interest are $4p^5 5s^2 4d(^3P)5d(^2P)$ at 30.80 eV and $4p^5 5s^2 4d(^3P)7s(^2P)$ at 31.10 eV. The $4p^5 5s^2 4d(^3P)6s(^2P)$ resonance lies over the $4p \rightarrow 4d$ resonances at 29.40 eV. Note that we have shown only the lower Rydberg resonances.

Our total $4d$ cross section for both length and velocity is given in Fig. 4 along with Hartree-Fock results. The discrepancy between length and velocity forms near

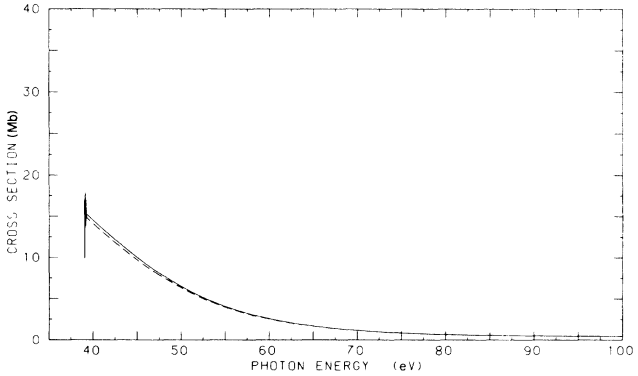

FIG. 8. The correlated total cross sections (sum of $4d$, $5s$, and $4p$ cross sections) in dipole length (solid line) and dipole velocity (dashed line) formalism in the region from 39.70 to 100.0 eV.

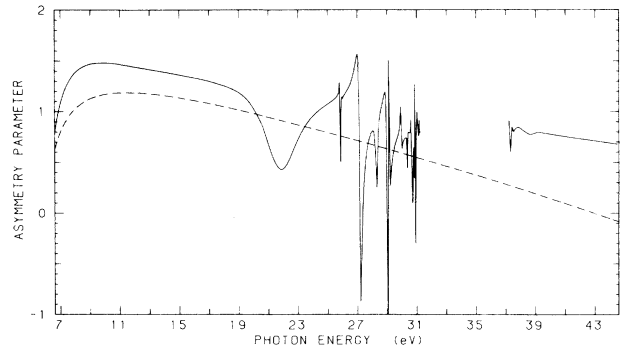

FIG. 9. Angular asymmetry parameter β for $4p^6 5s^2 4d \rightarrow 4p^6 5s^2 kf, kp$ excitations in the length formalism. The Hartree-Fock result is shown by the dashed line and the solid line is the correlated results. The dense region of Rydberg resonances which lies between 31.10 and 39.70 eV is not shown for the correlated result.

threshold could possibly be reduced by higher-order effects. We note the strong effect of the $4p \rightarrow 4d$ resonances. The dense region of Rydberg resonances which lies between 31.10 and 39.70 eV is not shown. There is a considerable effect on the partial cross sections discussed above due to the ground-state correlation diagrams of Fig. 1(c) and 1(e) with $p = 4d, k = kf$ (or kp) and $q = 4p, k' = 4d$. The tabulated $4p$ edges are given in Table I. In Table II we present numerical values for length and velocity results at higher energies. The difference between correlated cross sections and lowest-order (Hartree-Fock) cross sections becomes small at higher energies.

In Fig. 5 we present our total $5s$ cross section. Again there is a large effect due to the $4p \rightarrow 4d$ resonances. The tabulated positions of these resonances are given in Table III. Only the $4p^5 5s^2 4d^2 ({}^3F)^2 D$ resonance is shown in the dense region of Rydberg resonances. The cross section is small in the region beyond 39.70 eV. In Fig. 6 we show the total $4p$ cross section. Since length and velocity results are very close, only the length result is shown. The partial cross sections of $4p^5 5s^2 4dkd$ and $4p^5 5s^2 4dks$ were added to obtain the total $4p$ cross section shown in Fig. 6. There are 24 partial cross sections when all possible LS couplings for the ion $4p^5 5s^2 4d$ are considered. The final states including the continuum electron are ${}^2F$, ${}^2D$, and ${}^2P$. The threshold energies for $4p$ excitations are spread over the range 31.80–39.20 eV (Table I). In this region there are bound excitations $4p \rightarrow nd, ms$ ($n \geq 5, m \geq 6$) of a given channel which are degenerate with continuum $4p \rightarrow kd, ks$ excitations of other channels and give rise to resonances. These Rydberg resonances are not shown. In the region beyond 39.70 eV the total $4p$ cross section is larger than both the total $4d$ cross section and the total $5s$ cross section.

In Fig. 7 the total cross section (sum of $4p$, $4d$, and $5s$ cross sections) is presented. The resonances are the same as those shown in Fig. 5. The cross section in the region from 31.10 to 39.70 eV which is crowded with Rydberg resonances is not shown. In Fig. 8 we show the total cross section in the region from 39.70 to 100.00 eV.

TABLE IV. Angular asymmetry parameter β for the total $4d$ cross section. The symbols L and V refer to length and velocity formalism.

	Hartree Fock		Coupled equations	
ω (eV)	L	V	L	V
6.80	0.5184	0.4999	0.5163	0.5277
8.70	1.0653	1.0707	1.4021	1.4389
9.90	1.1529	1.1537	1.4813	1.5101
15.23	1.1371	1.1225	1.3903	1.5288
13.00	0.8351	0.8541	0.8435	0.7886
41.35	0.0970	0.1209	0.7547	0.6445
224.22	0.5692	0.5641	0.6878	0.6340
496.34	0.2353	0.2134	0.2758	0.2393
877.29	0.2371	0.2217	0.1660	0.1618
1965.76	0.4591	0.4479	0.3502	0.3515

The cross section is dominated by the total $4p$ cross section in this region.

In Fig. 9 we present the angular asymmetry parameter β in length form for the total $4d$ cross section. Length form results are given both in the Hartree-Fock approximation and including correlations. The velocity results are very close to the length results. The tabulated results for the β parameter are given in Table IV. The β parameter shows the resonance structure due to $4p \rightarrow 4d$ excitations. The resonance structure appearing between 31.10 and 39.70 eV is the Rydberg series due to $4p \rightarrow nd, ns$ excitations.

IV. DISCUSSION AND CONCLUSION

We have used many-body perturbation theory to calculate the photoionization cross section of neutral yttrium. By including correlations both in the ground state and in the final state we have found good agreement between length and velocity calculations The calculations predict prominent resonance structure due to $4p \rightarrow 4d$ excitations both in the $4d$ and $5s$ cross sections. The positions of the $4p \rightarrow 4d$ resonances were calculated approximately and may be changed when the higher-order excitation energies and other pair correlation energies[25] among $4p$ and $4d$ electrons are included more accurately. The only available solid-state experimental result[11] shows a broad peak in the region of $4p \rightarrow 4d$ atomic excitations, but appears to extend to higher energies than the resonances calculated in this work. Very recent data on the atomic vapor by Mansfield[12] give qualitative support to the calculations.

Our present correlated result at threshold could be improved by including additional second-order (in H_C) correlations as was done for other atoms.[26] An improved future calculation should include core polarization, relaxation, spin-orbit splitting, and double electron resonances.

ACKNOWLEDGMENTS

We thank the U.S. National Science Foundation for support of this work. We also thank Dr. S. Salomonson, Dr. S. L. Carter, and Mr. Cheng Pan for helpful discussions.

[1]J. P. Connerade, M. W. D. Mansfield, and M. A. P. Martin, Proc. R. Soc. London, Ser. A **350**, 405 (1976).
[2]R. Bruhn, B. Sontag, and H. W. Wolff, Phys. Lett. A **69**, 9 (1978).
[3]M. Ya. Amusia, V. K. Ivanov, and L. V. Chernysheva, J. Phys. B **14**, L19 (1981).
[4]R. Bruhn, E. Schmidt, H. Schröder, and B. Sontag, Phys. Lett. A **90**, 41 (1982).
[5]R. Bruhn, E. Schmidt, H. Schröder, and B. Sontag, J. Phys. B **15**, 2807 (1982).
[6]E. Schmidt, H. Schröder, B. Sontag, H. Voss, and H. E. Wetzel, J. Phys. B **16**, 2961 (1983).
[7]L. J. Garvin, E. R. Brown, S. L. Carter, and H. P. Kelly, J. Phys. B **16**, L269 (1983).
[8]P. H. Kobrin, U. Becker, C. M. Truesdale, D. W. Lindle, H. G. Kerkoff, and D. A. Shirley, J. Electron Spectrosc. Relat. Phenom. **34**, 129 (1984).
[9]E. Schmidt, H. Schröder, B. Sontag, H. Voss, and H. E. Wetzel, J. Phys. B **17**, 707 (1984).
[10]M. O. Krause, T. A. Carlson, and A. Fahlmann, Phys. Rev. A **30**, 1316 (1984).
[11]J. H. Weaver and C. G. Olson, Phys. Rev. B **14**, 3251 (1976).
[12]M. W. D. Mansfield (unpublished).
[13]Z. Qian, S. L. Carter, and H. P. Kelly, Phys. Rev. A **33**, 1751 (1986).
[14]K. A. Brueckner, Phys. Rev. **97**, 1353 (1955); *The Many-Body Problem* (Wiley, New York, 1959).
[15]J. Goldstone, Proc. R. Soc. London, Ser. A **239**, 267 (1957).
[16]H. P. Kelly, Adv. Theor. Phys. **2**, 75 (1968).
[17]E. R. Brown, S. L. Carter, and H. P. Kelly, Phys. Rev. A **21**, 1237 (1980).
[18]A. F. Starace, in *Handbuch der Physik XXXI,* edited by S. Flügge and W. Mehlhorn (Springer-Verlag, Berlin, 1982), p. 1.
[19]S. L. Carter and H. P. Kelly, J. Phys. B **11**, 2467 (1978).
[20]S. L. Carter and H. P. Kelly, Phys. Rev. A **24**, 170 (1981).
[21]M. Ya. Amus'ya, N. A. Cherepkov, and L. V. Chernysheva, Zh. Eksp. Teor. Fiz. **60**, 160 (1971) [Sov. Phys.—JETP **33**, 90 (1971)].
[22]C. E. Moore, *Atomic Energy Levels,* Natl. Bur. Stand. (U.S.) Circ. No. 467 (U.S. GPO, Washington, D.C., 1949), Vol. II.
[23]C. F. Fischer, Comput. Phys. Commun. **4**, 107 (1972).
[24]L. J. Garvin, E. R. Brown, S. L. Carter, and H. P. Kelly, J. Phys. B **16**, 1269 (1983).
[25]H. P. Kelly and A. Ron, Phys. Rev. A **4**, 11 (1971).
[26]J. J. Chang and H. P. Kelly, Phys. Rev. A **12**, 92 (1975).